Publication Year	2022
Acceptance in OA	2025-02-11T17:30:50Z
Title	Martian Atmospheric Thermal Structure and Dust Distribution During the MY 34 Global Dust Storm From ACS TIRVIM Nadir Observations
Authors	Vlasov, P., Ignatiev, N., Guerlet, S., GRASSI, Davide, Korablev, O., Grigoriev, Shakun, A., Patsaev, D., Maslov, I., Zasova, L., Luginin, M., Trokhimovskiy, A., Millour, E., Forget, F., Haus, R., Arnold, G., Montmessin, F.
Publisher's version (DOI)	10.1029/2022JE007272
Handle	http://hdl.handle.net/20.500.12386/35909
Journal	JOURNAL OF GEOPHYSICAL RESEARCH (PLANETS)
Volume	127

JGR Planets

RESEARCH ARTICLE
10.1029/2022JE007272

Special Section:
ExoMars Trace Gas Orbiter - One Martian Year of Science

Key Points:

- Atmospheric thermal structure and dust content on Mars are retrieved from Atmospheric Chemistry Suite Thermal InfraRed channel nadir measurements in the spectral range 7.7–16.7 µm
- The 2018 global dust storm covered the entire planet and caused an asymmetric heating of the atmosphere with a hotter southern hemisphere
- We observe a reduced diurnal contrast of surface temperatures and a changed contrast of atmospheric thermal structure during the storm

Supporting Information:

Supporting Information may be found in the online version of this article.

Correspondence to:
P. Vlasov,
pavel.vlasov@phystech.edu

Citation:
Vlasov, P., Ignatiev, N., Guerlet, S., Grassi, D., Korablev, O., Grigoriev, A., et al. (2022). Martian atmospheric thermal structure and dust distribution during the MY 34 global dust storm from ACS TIRVIM nadir observations. *Journal of Geophysical Research: Planets*, *127*, e2022JE007272. https://doi.org/10.1029/2022JE007272

Received 28 FEB 2022
Accepted 13 SEP 2022
Corrected 2 Oct 2022

This article was corrected on 2 OCT 2022. See the end of the full text for details.

Martian Atmospheric Thermal Structure and Dust Distribution During the MY 34 Global Dust Storm From ACS TIRVIM Nadir Observations

P. Vlasov[1], N. Ignatiev[1], S. Guerlet[2], D. Grassi[3], O. Korablev[1], A. Grigoriev[4], A. Shakun[1], D. Patsaev[1], I. Maslov[1], L. Zasova[1], M. Luginin[1], A. Trokhimovskiy[1], E. Millour[2], F. Forget[2], R. Haus[5], G. Arnold[5,6], and F. Montmessin[7]

[1]Space Research Institute of Russian Academy of Sciences (IKI), Moscow, Russia, [2]LMD/IPSL, Sorbonne Université, PSL Research Université, École Normale Supérieure, École Polytechnique, CNRS, Paris, France, [3]Istituto di Astrofisica e Planetologia Spaziali—Istituto Nazionale di Astrofisica, Rome, Italy, [4]Research School of Astronomy and Astrophysics, Australian National University, Canberra, ACT, Australia, [5]Institute of Planetary Research, DLR, Berlin, Germany, [6]Institute of Geoscience, University Potsdam, Potsdam, Germany, [7]LATMOS, Guyancourt, France

Abstract The Thermal InfraRed channel in honor of professor Vassili Ivanovich Moroz (TIRVIM) of the Atmospheric Chemistry Suite onboard ExoMars Trace Gas Orbiter has continuously monitored the Martian atmosphere from 13 March 2018 until 2 December 2019, covering almost a complete Martian Year (MY). In the nadir mode of observations, infrared spectra obtained by TIRVIM in the spectral range 600–1,300 cm^{-1} permit retrievals of vertical temperature profiles from the surface up to 60 km of altitude, surface temperatures and column aerosol optical depths. Here we report the retrieved atmospheric thermal structure and the column dust content during the global dust storm (GDS) of MY 34 monitored from $L_s = 182.2°$ to $L_s = 211.8°$ (Solar Longitude), capturing the evolution of the GDS and the response of the atmospheric thermal structure to the changing dust loading. The global storm caused asymmetric atmosphere heating, predominantly in the southern hemisphere, and changed diurnal contrast of atmospheric thermal structure. We also observe a reduced diurnal contrast of surface temperatures at the peak of the GDS.

Plain Language Summary The thermal radiation emitted by Mars in the spectral range 7.7–16.7 µm was measured by the Atmospheric Chemistry Suite Thermal InfraRed channel in honor of professor Vassili Ivanovich Moroz (ACS TIRVIM) onboard ExoMars Trace Gas Orbiter. The nadir spectra carry information about the temperature of the atmosphere at different altitudes thanks to a deep CO_2 absorption present around 15 µm. Also, the dust loading can be found from the 9-µm silicate absorption, and the surface temperature can be estimated at 7 µm where the atmosphere is mostly transparent. We follow the evolution of these parameters during the strong global dust storm of Martian Year (MY) 34 (2018). The peculiarity of the ACS TIRVIM data set is the exceptionally dense coverage providing a new look at this otherwise well-studied dust event.

1. Introduction

Long-term observation of the thermal structure of the Martian atmosphere by thermal sounding from orbit was in focus of the attention of many missions to Mars. The data collected from the Viking Infrared Thermal Mapper experiment onboard the Viking Orbiters (Martin et al., 1979), the Infrared Interferometer Spectrometer onboard Mariner-9 (Santee & Crisp, 1993; Zasova et al., 2001, 2002), the Thermal Emission Spectrometer onboard Mars Global Surveyor (Smith, 2004), the Thermal Emission Imaging System (THEMIS) onboard Mars Odyssey (Smith et al., 2003), the Planetary Fourier Spectrometer onboard Mars Express (MEx) (Giuranna et al., 2021; Grassi et al., 2005; Wolkenberg et al., 2020), and the Mars Climate Sounder (MCS) onboard Mars Reconnaissance Orbiter (MRO) (Kleinböhl et al., 2009), provided information about the vertical structure of the Martian atmosphere along with dust particles and water ice clouds distributions. These data advanced the understanding of the structure and dynamics of the atmosphere.

Dust and water ice particles take part in the radiative transfer in the atmosphere. They are involved in dust, water and CO_2 cycles on Mars. The dust cycle includes injection of the mineral particles into the atmosphere, their transport and subsidence on the surface, affecting all processes in the Martian atmosphere. The most remarkable manifestation of the dust activity are dust storms which have long been known from telescopic observations from Earth and by a series of orbiters and landers. Global dust storms (GDS) are the most important and impressive transient phenomena on Mars. GDS are also named as global dust events (GDE) or "planet-encircling dust storms" (Cantor, 2007). A GDS can actually be a combination of several local dust storms occurring simultaneously or sequentially and covering the entire planet during several weeks. A large amount of dust particles in the atmosphere dramatically changes surface and atmospheric parameters and strongly affects the thermal structure and dynamics of the Martian atmosphere. Despite numerous researches, global dust storms are still unpredictable phenomena so each new experiment can expand our understanding of the GDE nature.

Global dust events have been observed in various Martian Years (hereinafter MY): 1, 9, 10, 12, 15, 21, 25, 28, and 34 (e.g., Martin & Kieffer, 1979; Martin & Zurek, 1993; Shirley, 2015; Shirley et al., 2019). The GDS occur irregularly and each event is of great scientific interest. The latest GDE of MY 34 has been monitored by several spacecraft including MRO (Kass et al., 2019; Kleinböhl et al., 2020; Montabone et al., 2020), Mars Odyssey (Smith, 2019), MEx (Wolkenberg & Giuranna, 2021), and ExoMars Trace Gas Orbiter (TGO) (Aoki et al., 2019; Fedorova et al., 2020; Luginin et al., 2020). ExoMars TGO is a joint European Space Agency and Roscosmos space programme with the aim of comprehensive exploration of Mars, launched on 14 March 2016. It fully started its nominal scientific mission in March 2018 after several months of aerobraking. A key goal of the TGO mission is detecting trace gases in the Martian atmosphere and performing long-term monitoring of aerosol distribution, temperature and composition of the atmosphere (Vago et al., 2015). The low 400-km near-circular orbit of the TGO with 12 orbits per day provides dense coverage of measurements in terms of local time as well as sampling of the entire planet with the exception of the polar areas. Such coverage gives the opportunity for the orbiter instruments to observe in detail the GDS of MY 34, which started to grow as a regional storm at $L_s \approx 185°$ (Solar Longitude) and became global at $L_s \approx 193°$.

In this paper we present the evolution of the thermal structure of the Martian atmosphere, from the surface up to 60 km of altitude, along with the evolution of dust column opacity during the global dust storm of MY 34, as retrieved from nadir observations by the ACS TIRVIM spectrometer onboard TGO. Section 2 contains a description of the TIRVIM instrument with general information about the experiment, details of TIRVIM calibrated spectra and a description of the analyzed data set in the period from 26 May 2018 till 15 July 2018 which include the first month of the global dust event. The retrieval method for vertical temperature profile, surface temperature, and dust and water ice contents is described in Supporting Information S1 section with discussion of its characteristics. In Section 3 we present the main results of the global dust storm of MY 34. We summarize and discuss the major findings in Section 4.

2. TIRVIM Data

2.1. ACS TIRVIM Experiment

One of the instruments mounted on TGO is the Atmospheric Chemical Suite (ACS) designed by Space Research Institute (IKI) in Moscow (Russia). ACS is a set of 3 spectrometers (Near InfraRed, Middle InfraRed, and Thermal InfraRed) intended to observe the Martian atmosphere in solar occultation, nadir and limb geometry modes (Korablev et al., 2018). Our research focuses on Thermal InfraRed channel (TIRVIM) nadir observations.

TIRVIM is a Fourier-transform spectrometer based on a 2-inch double-pendulum interferometer with cryogenically-cooled detector, which is capable of operating both in nadir and in solar occultation modes (Shakun et al., 2018). TIRVIM stands for Thermal InfraRed channel (TIR) named after Professor Vassili Ivanovich Moroz. The instrument covers the 1.8–16 μm spectral range in total and the 5–16 μm (620–2,000 cm^{-1}) range in nadir mode of observations. The primary goal of TIRVIM in nadir mode is the long-term monitoring of atmospheric and surface temperatures and aerosol column densities. The spectral resolution of $\Delta\nu = 1.17\ \text{cm}^{-1}$ in nadir mode (see details in Section 2.2) is high enough to retrieve temperature profiles in the wide altitude range—from the surface up to 55–60 km—with the vertical resolution of the order of a few kilometers in the lower atmosphere. At warmest conditions on Mars the signal-to-noise ratio (SNR) of the instrument measurements can amount up to $\sim 10^3$ at a $\nu \approx 770\ \text{cm}^{-1}$ (Korablev et al., 2018).

2.2. Observations With TIRVIM in Nadir Geometry

The TIRVIM instrument has a number of predefined operation modes, which differ in the maximum optical path difference or the number of interferogram counts, the reference channel frequency or the speed of the mirror motion and the associated electronic filters. The signal on the detector, or the interferogram, is recorded with a path difference step of $\Delta x \approx 0.76$ μm (defined by the reference channel laser diode wavelength) at a rate equal to the reference channel frequency. In nadir observation geometry TIRVIM operated in three modes: (a) a standard nadir mode with about 26,000 points in a two-sided interferogram; (b) an onboard interferogram averaging by eight successive interferograms with the number of saved points reduced down to 20,480; and (c) a maximum path difference mode with the number of points about 129,000. In all these modes the reference channel frequency was set to 71.1 kHz, so that it takes 0.36 s to register a 26,000-point interferogram.

Routine nadir observations by TIRVIM started in the standard mode in the period 13–19 of March 2018, with about 9,000 measurements per orbit. Then, to reduce transmitted data volume and increase the signal-to-noise ratio, the onboard interferogram averaging mode was switched on. In this mode, for the most part, a number of measurements per orbit was of the order of 500, but sometimes measurement density was increased up to 1,000–1,650 measurements per orbit. In the period from 28 April to 23 May, due to a hardware error, namely hang up of the double pendulum motion controller, the quality data volume was significantly reduced, so that only few calibrated spectra per orbit may be valid, and this period was excluded from the analysis. Then the instrument was rebooted and operated successfully from 26 May, which coincided with the beginning of the development of the global dust storm on Mars, till 15 July 2018, when another hardware issue occurred. It was caused by a failure of the Stirling cryocooler and overheating of the detector, and the instrument was switched off to avoid its damage. Routine measurements started again on 1 September 2018, already again in a standard nadir mode (without onboard averaging), and with a new observation schedule: only 2 working days out of 7. It should save a limited lifetime of the Stirling cooler, which is approximately equal to 10,000 hr. Analysis of the data obtained with the onboard interferogram averaging demonstrated that this mode produced a considerable percentage of erroneous interferograms, which were not easy to distinguish immediately. It is explained by the fact that a simple interferogram alignment by maximum values, done by the onboard software before averaging, may sometimes be wrong in a path difference coordinates. It happens when the observed object changes considerably on the time scale required to do a set of measurements to be averaged by the onboard software.

In the onboard averaging regime, the onboard software calculated an average of eight adjacent interferograms (separately for forward and backward motion of the mirror) keeping 20,480 points aligned by their maximum values. The actual maximum of both individual and average interferograms is located approximately in the center, an exact position being slightly variable. For further processing and calibration, interferograms were cut down to 2N = 20,400 points to always ensure equal length of both wings (10,200 points). This interferogram length was chosen for processing all nadir observations to simplify a further analysis of the calibrated radiance spectra with a constant instrumental function. The spectral sampling is then equal to $\Delta\nu = (2\text{N}\cdot\Delta x)^{-1} = 0.64$ cm^{-1}. With Hamming apodization the spectral resolution defined as the full width at half maximum is equal to $1.82\cdot\Delta\nu = 1.17$ cm^{-1}.

A full field of view of the instrument is equal to 2.8°, which gives a 20 km footprint on the Martian surface from a distance of 400 km. In the single interferogram mode a smearing due to orbital motion of the spacecraft is negligible (3 km/s), while in averaging mode the field of view is additionally elongated by 20 km.

The TIRVIM instrument appears to have a source dependent phase function, and its radiometric calibration was done according to Revercomb et al. (1988). For this purpose as a rule every 40 observations of Mars (20 in each mirror motion direction) were interleaved with two observations of the cold space and the internal calibration blackbody. The noise equivalent spectral radiance reaches its minimum values in the interval 700–800 cm^{-1}, and is equal to 0.3 and 0.1 mW/m^2/sr/cm^{-1} for the single and averaging mode, respectively.

Figure 1a represents a variety of emission spectra measured by TIRVIM with interferogram averaging by eight in the range from 600 to 1,300 cm^{-1}. The set of spectra in the brightness temperature units shows the main details of the analyzed data. The spectral range from 650 to 780 cm^{-1} contains the 15 μm CO_2 absorption band whose shape is strongly dependent enough on the vertical pressure-temperature profile to be retrieved. The retrieval algorithm is described in detail in Supporting Information S1 section. The data from the part of the spectra in the range below 650 cm^{-1} is not considered due to the low signal-to-noise ratio.

The part of a spectrum in the range from 780 to 1,300 cm^{-1} predominantly depends on the temperature of the Martian surface and general contents of dust particles and water ice clouds in the atmosphere (Clancy et al., 2003; Wolff & Clancy, 2003). During dust storms a wide dust band is detected in this range with maximum extinction

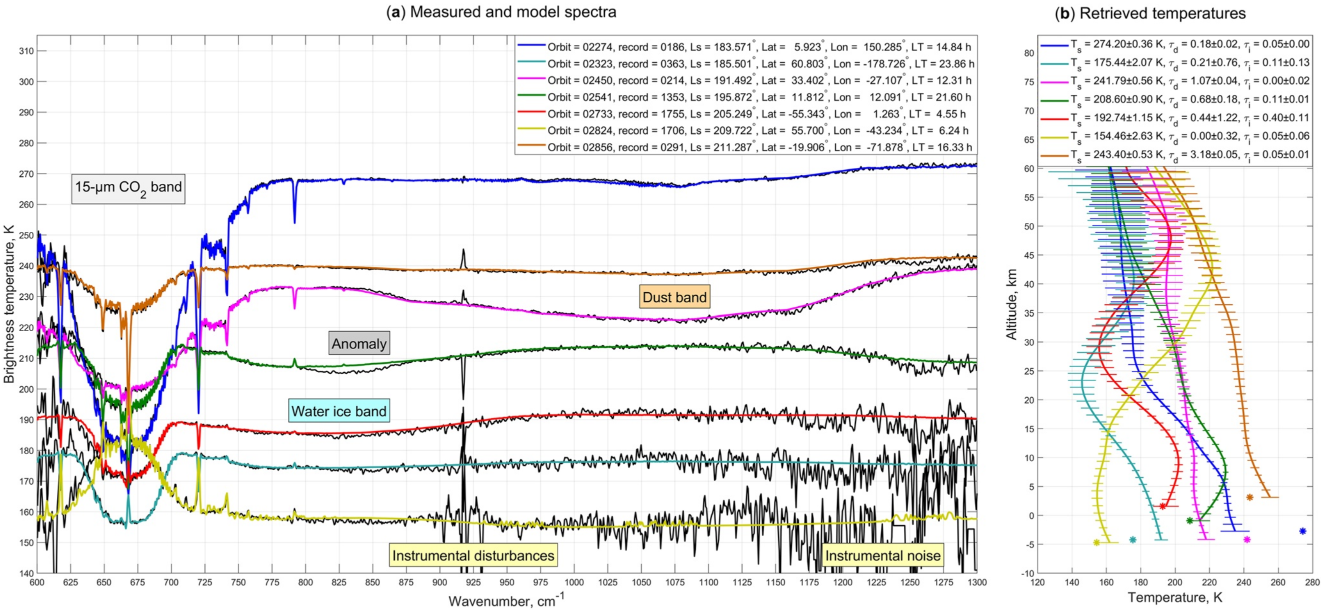

Figure 1. Examples of retrieved vertical temperature profiles from Thermal InfraRed channel in honor of professor Vassili Ivanovich Moroz (TIRVIM) measurements (b) during the first month of the global dust storm of Martian Year 34 and corresponding best fit simulated spectra (colored) compared to measured (black) ones (a). Surface temperatures T_s are shown by asterisk markers, column dust (τ_d at 1,075 cm^{-1}) and water ice (τ_i at 825 cm^{-1}) extinction optical depths are specified in the legend.

at ≈1,075 cm^{-1} (see Figure 1a, magenta). A water ice clouds absorption band is detected with maximum extinction at ≈825 cm^{-1} (see Figure 1a, red). A few weak CO_2 absorption lines in this spectral region and H_2O lines above 1,100 cm^{-1} can be neglected since their absorption doesn't affect the shape of a spectrum in general. The O_3 absorption lines at 950–1,100 cm^{-1} can be discounted as well due to the low ozone content. The brightness temperature in the range 780–800 cm^{-1} gives a good estimation of the surface temperature in the case of a pure atmosphere, taking the surface emissivity into account. Any significant dust and water ice loading may displace such an estimate from the real surface temperature by 10–20 K.

Some anomaly in the form of narrow absorption band is systematically detected in spectra in the range 800–900 cm^{-1} (see Figure 1a, green). The band is located in the region with water ice maximum absorption but being too narrow it is not simulated by any size particle distribution of water ice. We suppose an artificial origin of this absorption band which is caused by the instrument. The anomaly significantly complicates water ice content retrieval and affects column dust optical depth retrieval in some cases.

Also, the upper boundary (1,300 cm^{-1}) of the useful spectral range is reduced to lower wavenumbers to avoid incorrect interpretation of column dust optical depth during the retrieval process in the cases of low signal-to-noise ratio in this spectral region. For example, it is difficult to retrieve dust content for the morning observation at northern mid-latitudes with a cold surface (see Figure 1a, yellow). In some cases SNR at wavenumbers larger than 800 cm^{-1} is too small to retrieve dust and water ice content. Moreover, some systematic wave-like distortions in the range 1,000–1,300 cm^{-1} (see Figure 1a, green, red, cyan, and yellow) additionally complicate dust retrievals and enlarge errors especially in cases if dust band is shallow or is not observed.

An interval from 900 to 950 cm^{-1} is excluded from the analysis because of artificial spectral features caused by acoustic disturbances generated by the Stirling cryocooler of the instrument's detector. The shape and width of the disturbance peak varies across the data set so a spectral interval with some margin should be omitted.

Figure 1b represents examples of retrieved vertical temperature profiles along with surface temperatures and dust and water ice contents. Surface temperatures are displayed by asterisk markers, column dust and water ice extinction optical depths are specified in the legend. Measured (in black color) and best fit simulated spectra (colored with the same color as for corresponding retrievals) are shown in Figure 1a. The equatorial daytime temperature profile observed at $L_s = 183.6°$ before the GDS (Figure 1b, blue) is characterized by a hot surface (274 K) and colder air with decreasing temperature throughout the troposphere and tropopause. The nighttime thermal structure at northern polar latitudes at L_s = 185.5° (Figure 1b, cyan) reflects well-known dynamical "polar warming" at 40–45 km of altitude and 175 K surface colder than the lower troposphere.

Late morning observation at in the northern tropics at L_s = 191.5° during the onset of the dust storm (Figure 1b, magenta) shows almost monotonic decrease of vertical temperature profile with low gradient and hotter surface of 242 K. The corresponding spectrum contains deep dust absorption band centered at 1,075 cm^{-1}. The measurement performed by TIRVIM at late evening around the equator at L_s = 195.9° during the outbreak of the storm (Figure 1b, green) demonstrates temperature inversion in the lower troposphere and the dust band emission in the corresponding spectrum.

Nighttime vertical profile observed at L_s = 205.2° at the peak of the GDS close to southern polar latitudes (Figure 1b, red) is characterized by 2 temperature inversions—one in the lower troposphere and the other in the tropopause with the southern "polar vortex" between them. Corresponding spectrum contains a noticeable water ice band in the range 750–1,000 cm^{-1}. Morning thermal structure at L_s = 209.7° at higher northern mid-latitudes (Figure 1b, yellow) represents huge air temperature inversion throughout the whole troposphere, except the lower layers of the atmosphere, and cold surface of 154 K. The daytime measurement in the southern tropics at L_s = 211.3° (Figure 1b, brown) reveals monotonic decrease of air temperature from the surface up to mesosphere. Contrast between the surface temperature and air temperatures in the lower and middle troposphere is small and no dust band is observed despite high dust loading at the peak of the storm.

2.3. The Analyzed Data Set

In nadir mode ACS TIRVIM obtained $2.4 \cdot 10^6$ of spectra during the whole period of operation from 13 March 2018 till 2 December 2019 which covers the second half of the MY 34 from L_s = 142.8° and first half of the MY 35 up to L_s = 115.2°. In this paper we consider the period from 26 May 2018 till 15 July 2018 (from L_s = 182.2° to L_s = 211.8° of MY 34) which covers the first month of the global dust storm, and 49 complete sols in total. This data set doesn't cover the whole dust storm due to the overheating event of the detector that occurred on 15 July 2018. The next meaningful set of data did not begin to arrive until 1 September 2018. Thereby, the chosen period is the only opportunity to see the changing atmosphere during the evolution of the GDS of MY 34. Local time coverage of the data set can be seen in Figure 2.

The coverage of the measurements is rather dense due to continuous observation mode and the low (≈400 km of altitude) near-circular orbit of TGO which provides around 12 complete orbits around Mars per day. The data set contains 414 orbits (from #2252 till #2864) and 427,716 single measurements in total with interferogram averaging by eight. Each measurement represents a single emission spectrum in the range from 600 to 1,300 cm^{-1} with the latest version of calibrations. Emission angles are very close to zero due to nadir viewing from the nearly-circular orbit. There is a gap in the data due to a break of the measurements between L_s = 191.6° and L_s = 194.4°. We caution that though TIRVIM nadir measurements sample the full diurnal cycle in 54 sols, during the strong dust storm the thermal structure changes quite rapidly so only its instant state twice a day can be displayed.

3. Observations of the MY 34 GDS

3.1. Evolution of the Atmospheric Dust Spatial Distribution

In this section we describe the evolution of atmospheric dust spatial distribution retrieved from ACS TIRVIM measurements during the global dust storm of MY 34 in the period from L_s = 182.2° to L_s = 211.8°. Figure 3 represents latitudinal and seasonal variability of zonally and diurnally averaged total column dust extinction optical depth at 1,075 cm^{-1}. All retrievals are taken over a fixed period of time of 4° in terms of longitude solar, being acquired within ±2° of the considered L_s. The selected retrieved optical depths are binned in 4° latitude bins with diurnally averaging and averaging over all longitudes. The absence of measurements between L_s = 191.6° and L_s = 194.4° explains the gap in the seasonal dust map. Measurements that are too noisy in the range 950–1,300 cm^{-1} (mostly in polar regions) were filtered out to avoid unreliable dust optical depth retrievals.

According to Figure 3, the low dust loading in the atmosphere with τ_{dust} = 0.2–0.3 persists until L_s = 186° when the GDS of MY 34 starts. Due to the onset of the dust storm, a slight increase of the dust presence in the northern hemisphere is observed from L_s = 186° to L_s = 192°. Close to the data gap which began at L_s = 191.6°, the dust

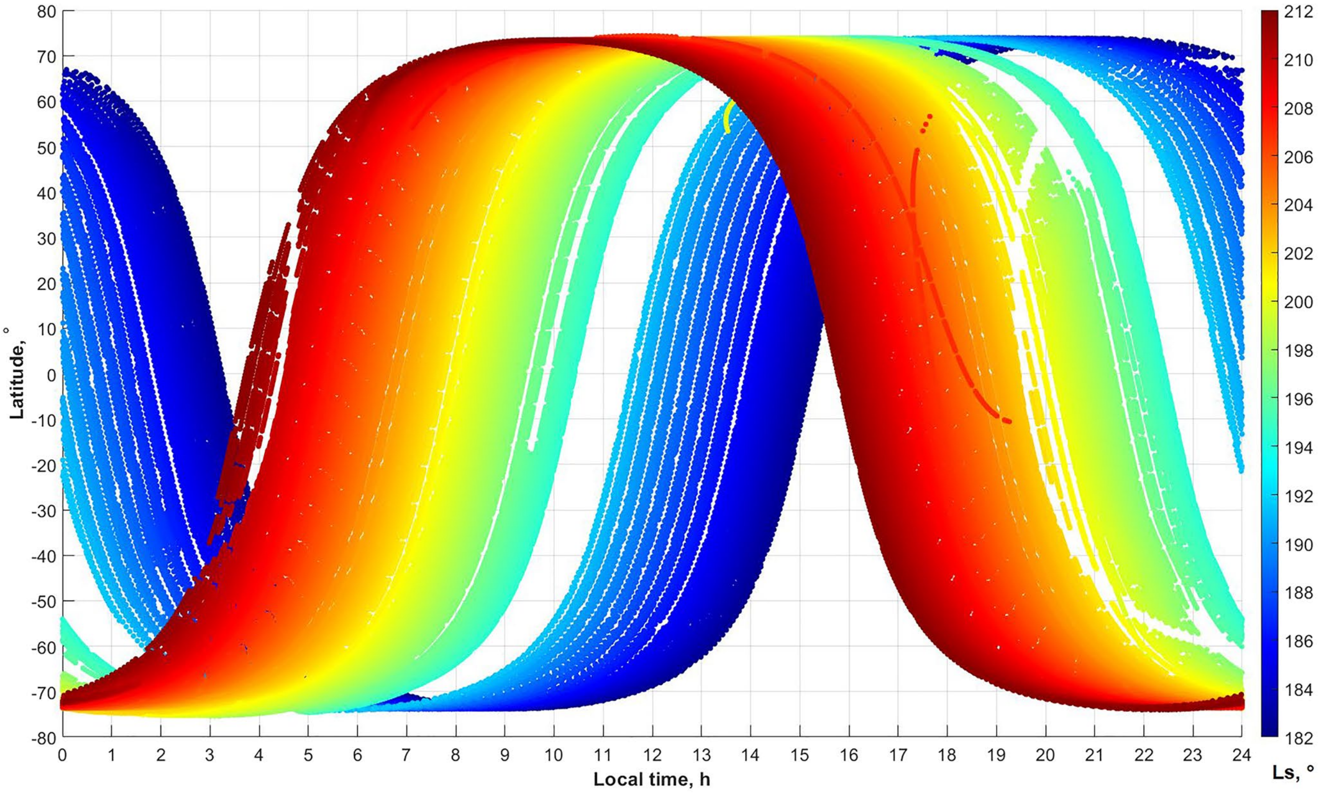

Figure 2. Colored latitude/local time coverage of Thermal InfraRed channel in honor of professor Vassili Ivanovich Moroz (TIRVIM) measurements in the period from 26 May 2018 till 15 July 2018 (L_s = 182.2°–211.8°) which covers the first month of the global dust storm of Martian Year 34.

loading expands up to 50°N and extends to 25°S, reaching values of ≈1 of zonal mean extinction optical depth at some latitudes. TIRVIM measurement coverage is insufficient to display the whole rapid process of the storm outbreak to southern latitudes before the short measurements break at L_s = 191.6°. We also don't see how the storm becomes global at L_s ≈ 193° due to the gap in the data. After the gap, the column extinction optical depth sharply increases southwards up to 60°S and reaches 1.5–2 with local maximum of ≈2.5 between 30°S and 10°N

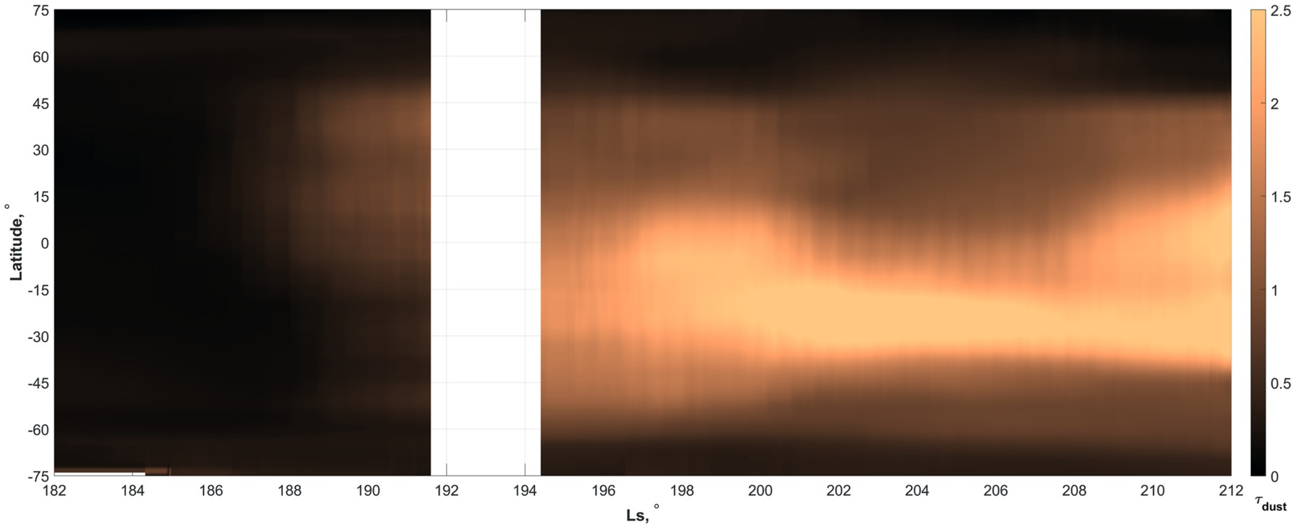

Figure 3. Zonal mean of the diurnally averaged column dust extinction optical depth at 1,075 cm^{-1} during the global dust storm of Martian Year 34 in the period from L_s = 182.2° to L_s = 211.8°.

at $L_s \approx 198°$, which is also observed by the THEMIS instrument onboard Mars Odyssey (Smith, 2019) by the MCS instrument onboard MRO (Kass et al., 2019; Montabone et al., 2020).

Some shift in the dust activity to the southern hemisphere between $L_s = 200°$ and $L_s = 208°$ is observed, while activity in the northern hemisphere is maintained at column optical depths values of 1–1.5. In the southern latitudes between 5°S and 35°S the column extinction optical depth at 1,075 cm^{-1} exceeds 2.5 at maximum. In the period from $L_s = 208°$ the atmospheric dust spreading again northwards with slight increase of optical depths to ≈2 and higher in latitudes from 40°S to 20°N can be observed. Thus, the GDS at its peak covers the entire planet from 60°S to 50°N. Such lack of column dust between $L_s = 200°$ and $L_s = 208°$ in the northern hemisphere is not observed neither by THEMIS nor by MCS and is caused by the degeneracy of the problem of dust retrieval from nadir observations with specific thermal structure in the lower atmosphere. As can be seen from the local time data coverage in Figure 2, in the period from $L_s = 200°$ to $L_s = 208°$ the significant part of measurements at equatorial and middle latitudes was made predominantly in the morning and evening hours with the surface temperature close to air temperatures at altitudes below three pressure scale heights where the bulk of the dust is located. Moreover, there are a lot of daytime observations after $L_s = 208°$ with similar thermal structure. Such low contrast between the surface temperature and air temperatures lead to barely noticeable dust absorption bands in nadir spectra at 9.3 μm and to systematically unreliable low and high dust content retrievals. It manifests not only in artificial narrowing of the dust storm core and lack of dust in northern latitudes but also in zones with too low values of column dust optical depth around the bulk (see Figure 4). The details of the degeneracy problem can be found in Supporting Information S1.

The set of images in Figure 4 shows spatial maps of evolution of column dust extinction optical depth at 1,075 cm^{-1} during the global dust storm of MY 34 in the period from $L_s = 182.2°$ until $L_s = 211.8°$. The retrieved optical depths are selected over a fixed period of time of 5° in terms of L_s for each spatial map, and then are binned in 4° latitude and 4° longitude bins with diurnally averaging. A wide rolling average window is used to display column dust depth maps due to the lack of continuous coverage for all coordinates at the same time. Thus, the data on individual panels in Figure 4 overlap. Since there is the data gap, it would be better to describe spatial dust distribution evolution separately. Images a and b in Figure 4 demonstrate the onset and outbreak of the GDS until $L_s = 191.6°$ where the data gap starts, and the set of spatial maps c–i represents further evolution of the dust storm in the period from $L_s = 194.4°$ until the end of the data set.

According to Figure 4a the core of the storm origin is located in the northern hemisphere around 10°N and between 50°W and 0° of longitudes arising at $L_s \approx 186°$. During the initial evolution of the storm the core expands in all directions with a branch in the northern hemisphere that extends eastwards. Toward the end of the period before the data gap, as it is shown in Figure 4b, the bulk of the dust is concentrated north of 15°S between 60°W and 45°E of longitudes with the dusty region up to 140°E at the northern mid-latitudes between 25°N and 50°N, while the dust particles are slightly spread in the southern hemisphere. Direct comparison of daily averaged column dust spatial maps shows good agreement with MCS observations (Montabone et al., 2020) during the onset and outbreak of the MY 34 GDS (see Figure S2 in Supporting Information S1).

The obtained results are also quite consistent with the Curiosity rover ground observations in the Gale Crater (4.5°S, 137.4°W). Curiosity measurements reveal a 12–14 times growth of column dust optical depth in the crater from $L_s = 190°$ to $L_s = 195.5°$ (Guzewich et al., 2019). TIRVIM observations did not cover the Gale crater region in the period from $L_s = 190°$ to $L_s = 191.6°$ and the instrument did not permit any measurements from $L_s = 191.6°$ to $L_s = 194.4°$ so the dust content can be tracked only after outbreak of the GDS. Panels a and c in Figure 4 show that observed by TIRVIM column dust optical depth has increased 10–15 times in this region in the period from $L_s \approx 189°$ to $L_s \approx 196°$ which is in good agreement with Curiosity rover ground observations taking into account averaging of retrievals from TIRVIM measurements in a wide seasonal range.

During the further evolution the dust storm shifts southward in the period from $L_s = 194.4°$ to $L_s = 199°$ and covers both hemispheres between 60°S and 50°N (Figure 4c). From $L_s = 199°$ the active core of the GDS with column optical depths in the range 2–3 spreads into all longitudes and covers the entire planet mainly at equatorial latitudes and southern mid-latitudes (Figure 4d). After $L_s = 201°$ the core of the storm begins to narrow down and concentrate in the southern hemisphere (panels e–g in Figure 4) with reverse expansion back to the northern hemisphere from $L_s = 209°$ (panels h and i). Further comparison with MCS observations (Montabone et al., 2020) exhibits significant discrepancy between TIRVIM and MCS measurements after $L_s = 200°$

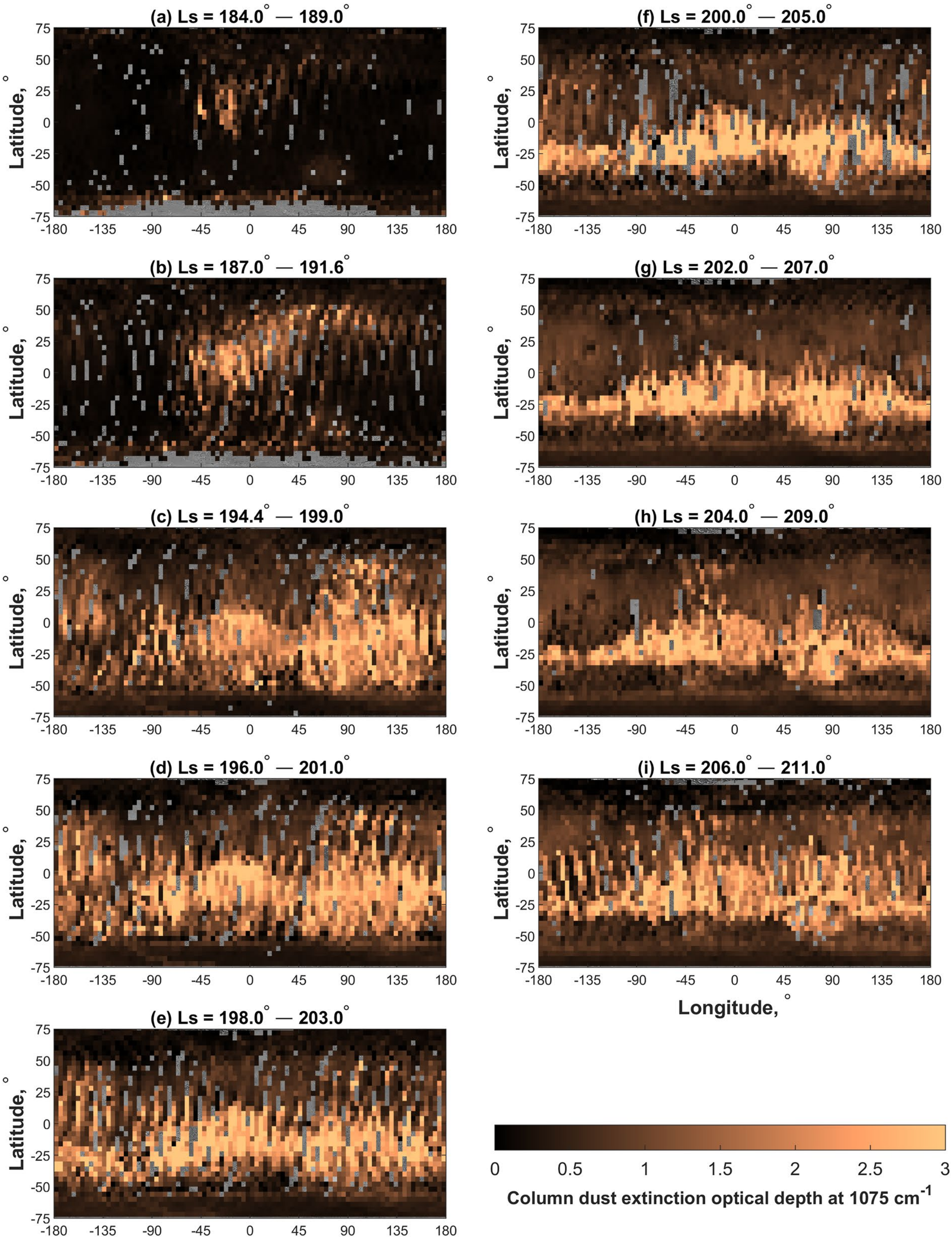

Figure 4. The evolution of the global dust storm of Martian Year 34. The diurnally averaged spatial maps of column dust extinction optical depth at 1,075 cm^{-1} in the periods: (a) from L_s = 184.0° to L_s = 189.0°, (b) from L_s = 187.0° to L_s = 191.6°, (c) from L_s = 194.4° to L_s = 199.0°, (d) from L_s = 196.0° to L_s = 201.0°, (e) from L_s = 198.0° to L_s = 203.0°, (f) from L_s = 200.0° to L_s = 205.0°, (g) from L_s = 202.0° to L_s = 207.0°, (h) from L_s = 204.0° to L_s = 209.0°, (i) from L_s = 206.0° to L_s = 211.0°.

while daily averaged dust spatial maps still agree well with each other during the period from $L_s = 194°$ to $L_s = 200°$ (see Figure S2 in Supporting Information S1). Such significantly different spatial column dust distributions at L_s after 200° are caused by the degeneracy mentioned above and discussed in detail of Supporting Information S1.

3.2. Evolution of the Thermal Structure of the Atmosphere

Here we describe the evolution of the atmospheric thermal structure throughout the GDS of MY 34 from $L_s = 182.2°$ until $L_s = 211.8°$. The temperature fields in the form of meridional cross-sections of the thermal structure shown in Figure 5 are formed by binning all retrieved temperature profiles taken over a fixed period of time (5° in terms of longitude solar was found to be a good choice) with averaging over all longitudes. The evolution of the thermal structure shown within overlapped ranges of L_s is tracked at 2 local times spaced by a half-day. Figure 2 with the local time coverage of the data set indicates that in order to display a latitude range as wide as possible (from 70°S to 70°N) we should bin all retrieved temperature profiles acquired within ±3 hr from the considered local time. Local times of the displayed night-morning and day-evening occurrences drift slightly with the season because of incomplete local time coverage. By analogy with the spatial column dust optical depth distribution results section, because of the data gap it would be better to separate thermal structure evolution description into two parts: a period of initial heating of the atmosphere from $L_s = 182.2°$ to $L_s = 191.6°$ (Figure 5a and 5b) and a period of strong asymmetric heating caused by dust particles ejection into the atmosphere from $L_s = 194.4°$ to $L_s = 211.8°$ (Figures 5c–5i). The local time difference between the consequent plots of Figure 5 is much smaller than the binning window, so the evolution in terms of L_s can be tracked adequately.

Figure 5a with display of a nearly dust-free atmosphere at 2 and 14 hr of local time reflects the well-known seasonal mean meridional cross-sections of Martian atmosphere at northern fall equinox during the night and day consequently (McCleese et al., 2010). Both structures demonstrate strong latitudinal gradients of temperature from middle latitudes into polar regions at lower troposphere with sharper gradient at southern polar latitudes and nearly invariability of the temperature near the equator. Near-surface atmospheric temperatures reach 220–225 K around the equator and at middle latitudes. A monotonic decrease of the temperature from near-surface layers throughout the troposphere is observed at the equator and middle latitudes except for the polar regions. The equinoctial Hadley circulation with nearly symmetric cells around the equator leads to a dynamical warming of ≈175 K in the tropopause (≈50 km of altitude) at the polar regions of both hemispheres and to nearly symmetric cold "polar vortices" of ≈150 K in the middle troposphere (French & Gierasch, 1979). The obtained "polar warmings" are not as marked as observed by MCS onboard MRO (Kleinböhl et al., 2020) due to wide averaging of TIRVIM measurements (within ±3 hr) as well as low sensitivity and worse vertical resolution of retrievals (≈20 km) at ≈50 km of altitude compared to ∼5 km by MCS. In general the agreement with MCS observations is of the order of temperature retrieval errors (see Supporting Information S1).

Figure 5b demonstrates initial heating of the atmosphere at the onset of the MY 34 GDS with vertical growth of the temperature from the surface up to high altitudes. An absorbing of solar radiation by atmospheric dust in the northern hemisphere (as shown in panels a and b of Figure 4) caused a daytime heating up to ≈10 K on average in the middle troposphere at latitudes with GDS core location and associated increase in nighttime temperatures. The spreading of the temperature by descending branches of Hadley circulation also heats the "polar warmings." Near-surface temperatures are maintained in all the latitudes at both times of day.

Images c and d in Figure 5 represent the thermal structure of a warmed-up atmosphere at 8 and 20 hr of local time in the period from $L_s = 194.4°$ to $L_s = 201.0°$ after the measurements break when the storm has already expanded into a global. The semidiurnally separated thermal structures become very dissimilar, in contrast to the ones before the GDS. The morning temperature field is nearly symmetric relative to the equator with temperatures 220–225 K at altitudes below 30 km. The southern polar region at 8 hr is characterized by the slight temperature inversion from the surface up to ≈10 km at latitudes south of 50°S as well as ≈180 K tropopausal "polar warming" which is wider and hotter than during the initial heating before $L_s = 191.6°$. Another morning inversion from 20 to 40 km north than 50°N is well-observed with the heating branch stretched to the northern polar region above 30 km with temperatures more than 190 K and caused by the equinoctial Hadley circulation. As for the evening temperature field, the thermal structure at 20 hr is characterized by an asymmetric huge warm zone with temperatures above 190 K below 40 km between 60°S and 50°N with slight equatorial minimum at all altitudes above 10 km. The evening thermal structure reflects the latitudinal asymmetry in the heating of the atmosphere by the solar radiation absorption by dust particles during the day, with dust dominating in the equatorial region

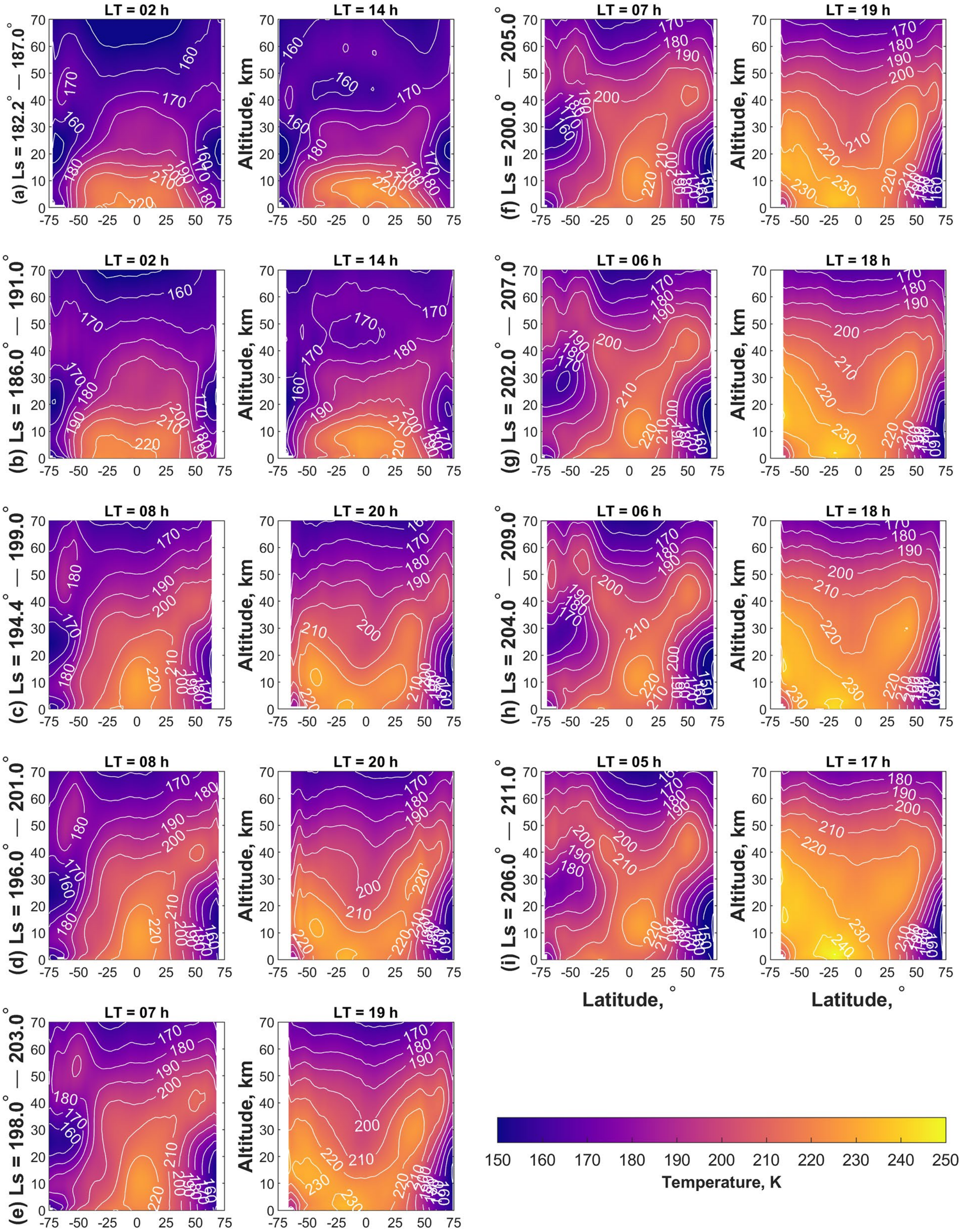

Figure 5. Mean meridional cross sections of retrieved thermal structure up to 70 km during the global dust storm of Martian Year 34 in the periods: (a) from $L_s = 182.2°$ to $L_s = 187.0°$, (b) from $L_s = 186.0°$ to $L_s = 181.0°$, (c) from $L_s = 194.4°$ to $L_s = 199.0°$, (d) from $L_s = 196.0°$ to $L_s = 201.0°$, (e) from $L_s = 198.0°$ to $L_s = 203.0°$, (f) from $L_s = 200.0°$ to $L_s = 205.0°$, (g) from $L_s = 202.0°$ to $L_s = 207.0°$, (h) from $L_s = 204.0°$ to $L_s = 209.0°$, (i) from $L_s = 206.0°$ to $L_s = 211.0°$. All retrieved temperature profiles from the selected periods of L_s acquired within ±3 hr of the considered local time were averaged into bins of 2° of latitude and 1 km of altitude (above the areoid).

and southern middle latitudes and as a result hotter air in the southern hemisphere. The Hadley circulation forms branches of heating which are stretched to the troposphere with more distinct northern branch caused by initial presence of dust in the northern hemisphere before the storm expanded into global. Near-surface temperatures in the evening reach the maximum ≈230 K around 20°S.

Set of images e–i in Figure 5 shows further heating of the atmosphere at the peak of the GDS as morning and evening temperature fields: at 7 and 19 hr of local time in the period from L_s = 198.0° to L_s = 205.0°, at 6 and 18 hr from L_s = 202.0° till L_s = 209.0° and at 5 and 17 hr from L_s = 206.0° to L_s = 211.0°. The Hadley circulation continues to transport heat from the lower troposphere into the tropopause and mesosphere in both hemispheres. As a result, the night-morning northern inversion becomes more distinct and equatorial local temperature maximum of more than 220 K shifts upward from the surface up to 10–15 km of altitude. Moreover, the southern cold "polar vortex" is heated up to 170–180 K close to the end of the period and the "polar warming" of 200 K ceases to be separated. At daytime-evening hours the whole troposphere continues to significantly heat up due to the absorption of solar radiation by atmospheric dust particles during the day in equatorial and southern middle latitudes with heaviest dust loading. Close to the end of considered L_s the temperature field at 17 hr is characterized by hot values of more than 200 K throughout the troposphere and hotter than 220 K below 40 km of altitude in all latitudes between 60°S and 20°N with local maxima of 240–250 K in the southern hemisphere. Both morning and evening temperature fields are characterized by significant latitudinal gradients from 40°N into the North Pole in the lower troposphere. Again, the agreement of retrievals from TIRVIM nadir measurements with MCS/MRO observations at the peak of the GDS (Kleinböhl et al., 2020) is of the order of temperature retrieval errors (see Supporting Information S1). But, unlike the MCS instrument, TIRVIM sees the atmosphere under a heavy dust loading and provides information of its thermal condition below 20–30 km in the equatorial region and southern middle latitudes at the peak of the GDS.

3.3. Seasonal and Diurnal Temperature Contrasts

Figure 6a represents huge seasonal differences over a period of only 46 sols (25° in terms of L_s) between thermal structures before and at the peak of the GDS. Thermal changes are caused both by asymmetric heavy dust injection into the atmosphere and start of season shifting from equinoctial to solstitial. At the nighttime (3 hr) an extensive warming zone up south than 50°S below 40 km with temperature increase up to 40 K and noticeable region with cooling by ∼ 20 K at northern latitudes in the lower troposphere reflect predominantly seasonal changes from L_s = 180° to L_s = 225° (McCleese et al., 2010) rather than dust affect. In contrast, a warming in the higher troposphere and tropopause is caused by descending branches of Hadley circulation which spread the temperature from heated atmospheric layers during the GDS. The two marked maxima of temperature are centered on 30°S at 50 km of altitude with heating up to 40 K and on 45°N at 45 km with warming up to 50 K compared to the atmosphere before the GDS.

At the daytime (15 hr) the entire thermal structure below 70 km of altitude except the lower troposphere north than 25°N is the one huge region of heating compared to the atmosphere before the storm. Dust absorption of solar radiation during the day causes strong heating in the middle and upper troposphere. On the other hand, during the dust storm the lower layers of the troposphere receive less solar radiation which lead to slight cooling. Heating in tropopause and higher is caused by descending branches of Hadley circulation. In addition, the seasonal effect is also superimposed on the temperature changes at daytime caused by dust presence, similar to that at nighttime. The equinoctial Hadley circulation starts to changing into northern winter solstitial circulation mode causing a warming below 40 km in the southern hemisphere with temperature increase up to 40 K and cooling by ≈20 K in the northern lower troposphere similar to nighttime seasonal changes from L_s = 180° to L_s = 225° (McCleese et al., 2010). As a result, at the northern latitudes without heavy dust loading the structure changes are similar to nighttime. At latitudes south than 40°N thermal effects caused by heavy dust presence in the atmosphere significantly dominate over ones caused by seasonal change. In general, joint effect of reinforced Hadley circulation and asymmetric dust spatial distribution after L_s = 193° form global maximum of atmosphere heating up to 80 K around 60°S at 20–30 km of altitude.

Figure 6b shows diurnal average of the mean meridional thermal structure of the atmosphere $T_{\text{avg}} = 0.5\cdot(T_{15h} + T_{03h})$ before the onset of the GDS and at its peak, where T_{15h} is daytime temperature at 15 hr of local time and T_{03h} is nighttime temperature at 3 h. Figure 6c shows the diurnal contrast of the mean meridional thermal structure $T_{\text{diff}} = 0.5\cdot(T_{15h} - T_{03h})$ between 15 and 3 hr before the global storm and at its peak. The semidiurnal difference between day and night mean meridional temperature fields in the period from L_s = 182.2° to L_s = 187.0° before

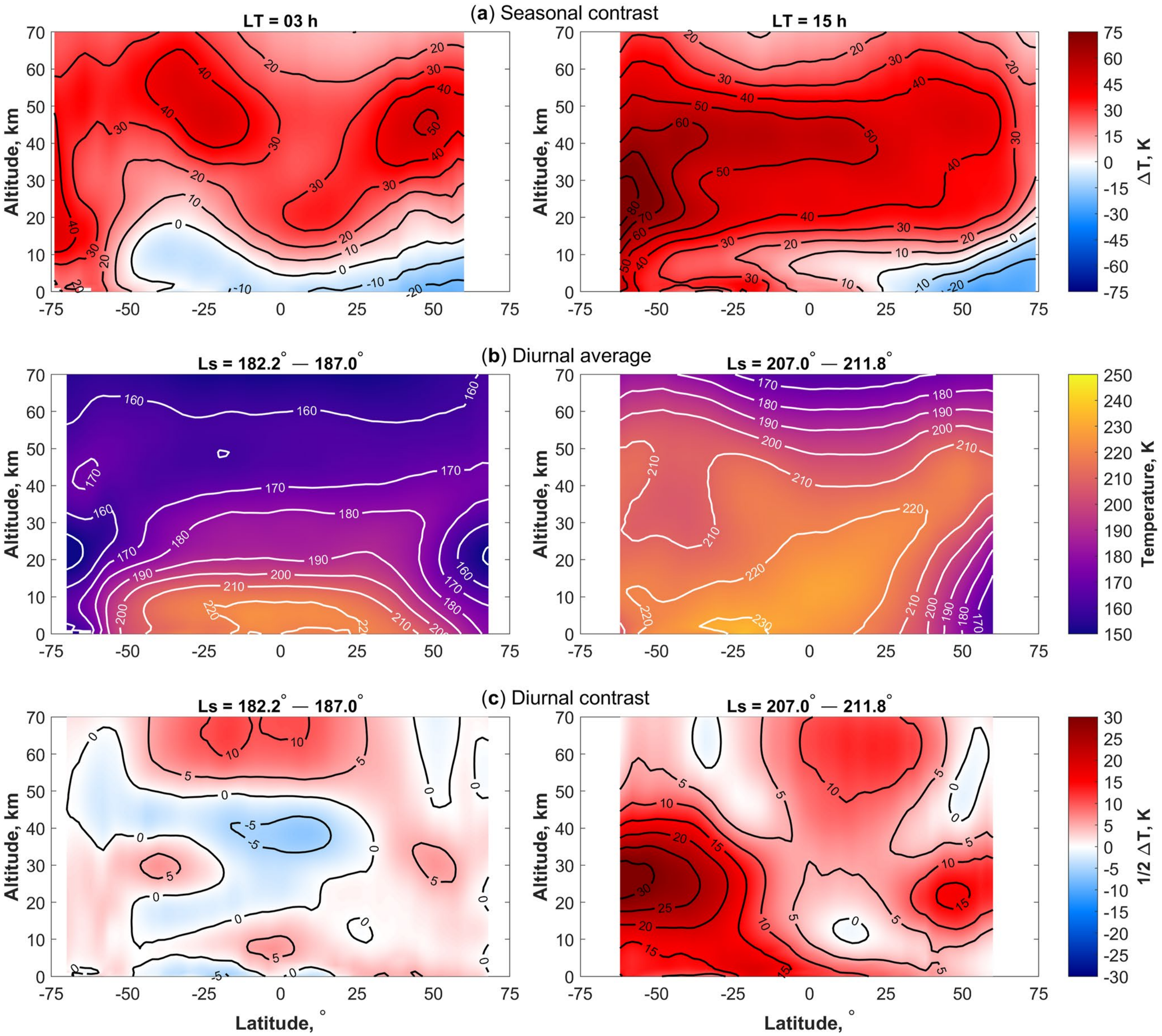

Figure 6. Mean meridional cross sections of (a) the difference of thermal structures between 182.2° and 187.0° (before the storm) and 207.0°–211.8° (the peak of the storm) of L_s at 3 hr (left) and 15 hr (right); (b) the diurnal average thermal structures $T_{\mathrm{avg}} = 0.5{\cdot}(T_{03h} + T_{15h})$ in 182.2°–187.0° of L_s (left) and 207.0°–211.8° of L_s (right); (c) the diurnal contrast of thermal structures $T_{\mathrm{diff}} = 0.5{\cdot}(T_{15h} - T_{03h})$ between 15 and 3 hr of local time in 182.2°–187.0° of L_s (left) and 207.0°–211.8° of L_s (right). All retrieved temperature profiles from the selected periods of L_s acquired within ±3 hr of the considered local time were averaged into bins of 2° of latitude and 1 km of altitude (above the areoid).

the storm represents a well-known thermal pattern typical for the equinox. This structure reflects forcing by the diurnal thermal tide and has been documented before from MCS measurements (Lee et al., 2009) and has been observed by the MCS instrument at the beginning of the MY 34 GDS as well (Kleinböhl et al., 2020). Equatorial deviations of the temperature with a region of cooling by 10–15 K centered at 30–45 km of altitude and semidiurnal temperature increase by 20–25 K above the tropopause (≈50 km) demonstrate vertically propagating diurnal tide in the equatorial region. Another equatorial region with night colder than day by 10 K is centered at 10 km of altitude. This pattern changes at 25–30° of latitudes with temperature increases of 10–15 K located at ≈30 km at 45–50° in both hemispheres. The sensitivity is not enough to retrieve structure above 60–70 km especially close to polar latitudes. Deviations in the other regions are of the order of temperature retrieval errors.

On the other hand, the thermal structure semidiurnal difference at the peak of the MY 34 GDS in the period from $L_s = 207.0°$ till $L_s = 211.8°$ is much more significant and asymmetric. The nodal pattern of the temperature difference with the equinoctial diurnal tide is no longer observed. The intensity of the mean meridional circulation and its vertical extent are stronger during the MY 34 GDS than before the storm or at the same season in Martian Years without GDS (Kleinböhl et al., 2020; Montabone et al., 2020). The strongest semidiurnal heating up to 60 K from nighttime to daytime is detected in the southern middle troposphere. Temperature deviations in the northern troposphere are represented by a region centered at 40–45°N and 20 km of altitude with air 30 K hotter during the day. Another zone with day warmer than night by 20 K is located in the northern tropopause and seems to be a seasonal pattern typical for $L_s = 225°$. Such structure due to the migrating diurnal tide is predicted by models (Wilson & Richardson, 2000) and has also been observed during MY 25 GDS (Guzewich et al., 2014). Regions where daytime and nighttime temperatures of the atmosphere are almost the same are represented by a small area around 15°N centered at 10–15 km of altitude and two zones at 35°S and 55°N located in the tropopause and above. The obtained tidal structure from TIRVIM observations during the storm confirms the MCS measurements with excellent agreement (Kleinböhl et al., 2020) though southern amplitudes observed by TIRVIM are 5 K stronger in general.

3.4. Diurnal and Seasonal Surface Temperature Variations

The dust injected into the Martian atmosphere takes part in the processes of radiative transfer and it is strongly involved in the heat balance of the planet during the global storm, affecting not only the temperature of the atmosphere but also the temperature of the Martian surface. Figure 7 represents the surface temperatures before the storm and at the peak of the GDS at 3 hr (left panels) and 15 hr (right panels) with demonstration of the dust influence. During daylight hours the atmospheric dust absorbs some part of the incident solar radiation, which leads to the lack of radiation received by the planet's surface and its cooling compared to dust-free conditions. At the peak of the storm the surface is 20–50 K colder on average than in the beginning of the GDS between 50°S and 50°N with a minimum of 60 K of decrease in some regions. Northern polar region cooled slightly less with ≈20 K of decrease at 15 hr. A sharp latitudinal gradient of the surface temperature at 55–60°S in a low-dust atmosphere and its absence at the peak of the storm lead to the fact that in the southern polar regions the surface during the day is even heated.

On the other hand, at dark time of day an increased backscattering of surface thermal emission from injected dust particles and radiation from the heated atmosphere hits the Martian surface and slows down its cooling during the night which leads to increase of the mean nighttime surface temperature. As a result, at the peak of the global dust storm the surface is 10–30 K warmer on average in latitudes between 60°S and 35°N with a maximum of 45 K of increase in some areas. At the same time there is slight cooling of the surface up to 15 K in the polar regions at 3 hr.

The retrieved spatial map of night heating is in good agreement with results of the General Circulation Model (GCM) simulations (Forget et al., 1999) assimilated with global column dust spatial distribution from MCS measurements (Streeter et al., 2020). The surface warming region (Figure 7c, left) coincides with the region where the bulk of the MY 34 GDS evolves at its peak (see Figure S2 in Supporting Information S1 with TIRVIM and MCS comparison of GDS spatial evolution), but we don't see correlation of nightside warming intensity with column dust optical depth and Mars topology. According to Streeter et al. (2020), the greatest relative nighttime warming areas are determined by surface radiative properties in dust-free atmosphere more than by dust loading during the storm. These regions are easily seen on Figure 7a (left) as coldest locations in dark violet colors. At 15 hr we don't observe such correlation of the daytime cooling with column dust optical depth as described in Streeter et al. (2020) and in general the retrieved temperature drop is ≈20 K stronger than simulated with GCM. The wide range of local time averaging of retrievals (within ±3 hr of the considered local time) from TIRVIM measurements should be taken into account. As well as the fact that we compare surface temperatures between $L_s = 182.2°–187.0°$ and $L_s = 207.0°–211.8°$ seasons of MY 34 instead of comparing seasons in the range $L_s = 200°–220°$ between MY 30 (without GDS) and 34 as been made in Streeter et al. (2020).

The obtained results are quite consistent with the Curiosity rover ground measurements (Guzewich et al., 2019) in the Gale Crater. According to Curiosity observations the surface temperature at 5 hr in the Gale Crater (4.5°S, 137.4°W) has been rosen by ≈20 K during the MY 34 GDS. Our retrievals show a growth of the surface temperature averaged in the range 0–6 hr by 20–25 K in the region with the Gale Crater. At the same time, the retrieved from TIRVIM measurements and averaged in the range 12–18 hr daytime cooling of the surface by 40–45 K is a little stronger than observed by the Curiosity drop of the temperature by ≈35 K in the range 12–13 hr caused

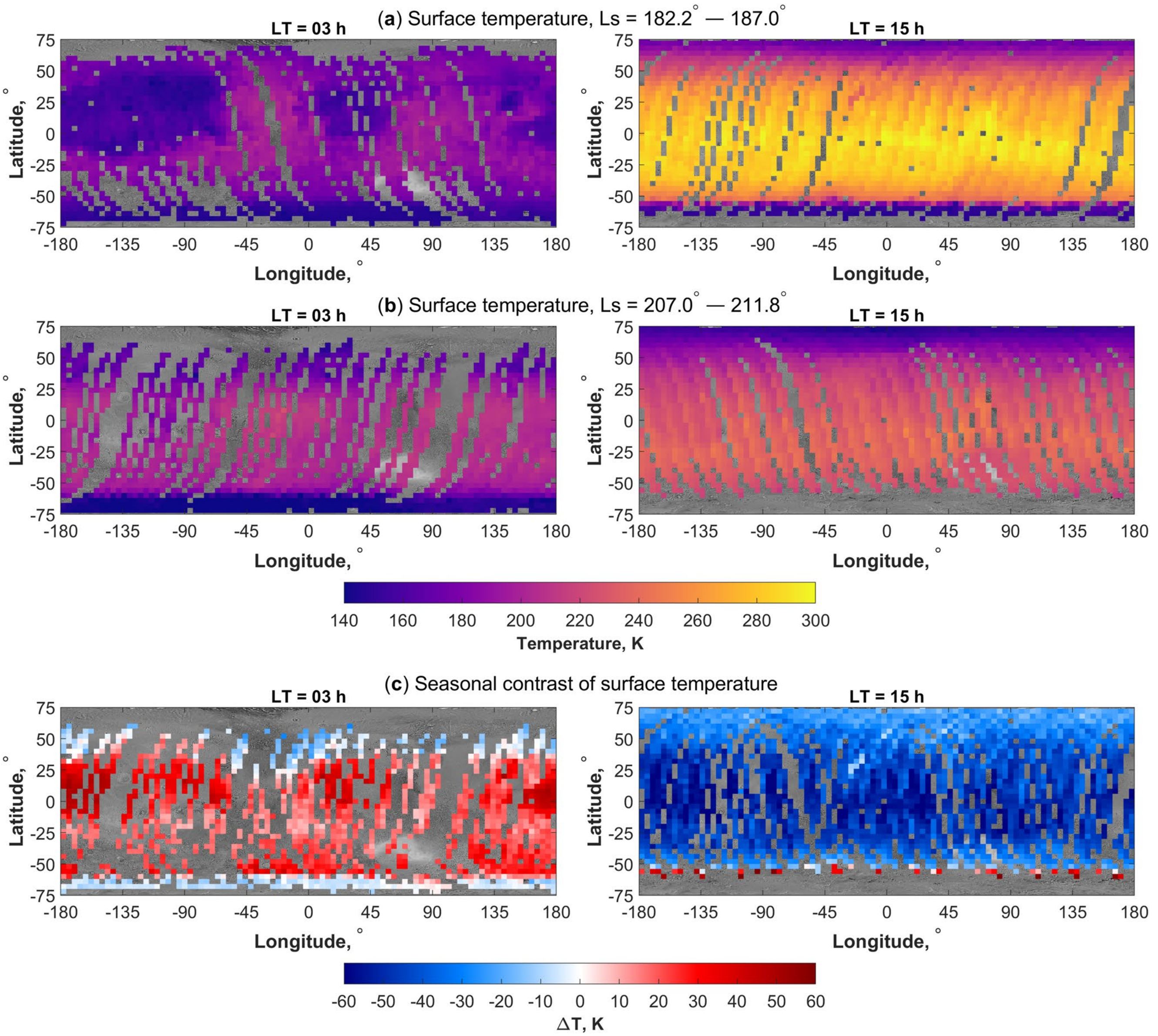

Figure 7. The temperature of the Martian surface at 3 hr (left) and 15 hr (right) of local time in the periods: (a) before the global dust storm from $L_s = 182.2°$ to $L_s = 187.0°$ and (b) at the peak of the storm from $L_s = 207.0°$ to $L_s = 211.8°$; (c) the seasonal difference between two considered seasons at 3 and 15 hr.

by the injected dust. In general, taking into account geographical averaging of retrievals from TIRVIM measurements and a wide range of local time averaging, obtained results show a quite good agreement with the Curiosity ground observations.

4. Summary

Being a part of ExoMars TGO, the ACS TIRVIM spectrometer has monitored the Martian atmosphere covering almost a complete MY. During its operation, ACS TIRVIM has continuously observed the first month of the global dust storm of MY 34 from 26 May 2018 till 15 July 2018 covering the period from $L_s = 182.2°$ until $L_s = 211.8°$ (almost 49 sols) with a short break from $L_s = 191.6°$ to $L_s = 194.4°$. Atmospheric temperatures as a function of height from the surface up to 60 km of altitude, surface temperatures and column dust and water ice optical depths were retrieved from nadir TIRVIM spectra in order to explore the atmosphere during the storm. In this paper, we analyzed mean meridional cross-sections of temperature and dust column optical depth maps at 1,075 cm^{-1} spaced at 4–5° of L_s. The dense ACS TIRVIM observations of the storm at different local times permit to look at this otherwise well-studied dust event from a new perspective. We were able to trace the change of the thermal structure at night-morning and day-evening hours during the strong injection of dust particles into the atmosphere.

As seen by TIRVIM, low dust loading in the atmosphere with $\tau_{\text{dust}} = 0.2–0.3$ persists until the GDS has begun at $L_s \sim 186°$ in the northern hemisphere near the equator as a local dust storm and then its core has expanded in all directions with a branch in the northern hemisphere that extends eastwards. Close to the short break of TIRVIM measurements at $L_s = 191.6°$, the high dust loading expands up to 50°N and extends to 25°S, reaching ≈1 of zonal mean extinction optical depth at some latitudes. It is not observed by TIRVIM how storm becomes global at $L_s \approx 193°$ due to the data gap but further measurements show that values of the column extinction optical depth sharply increase southwards up to 60°S and reach 1.5–2 with local maximum of ≈2.5 between 30°S and 10°N at $L_s \approx 198°$ with spreading of the storm core into all longitudes and covering the entire planet. The retrieved dust spatial distribution before $L_s = 200°$ is in good agreement with the THEMIS measurements onboard Mars Odyssey and the MCS observations onboard MRO.

In the period from $L_s = 200°$ to $L_s = 208°$ the most of TIRVIM measurements at equatorial and middle latitudes was made predominantly in the morning/evening as well as daytime hours after $L_s = 208°$ with observed low contrast of temperature between surface and air at altitudes where the bulk of the dust is located. Such thermal structure lead to barely noticeable dust absorption bands in nadir spectra at 9.3 μm even with heavy dust loading at the peak of the GDS and to unreliable low and high column dust depth retrievals. The problem of column dust depth retrieval becomes degenerate, when large variations in dust content lead to weak changes in a modeled emission spectrum, and this is a limitation of the very method of nadir observations of a similar thermal structure. As a result, a significant discrepancy of TIRVIM column dust spatial maps compared to MCS after $L_s = 200°$ is observed which manifests in artificial narrowing of the dust storm core and lack of dust in northern latitudes between $L_s = 200°$ and $L_s = 208°$as well as in zones with too low values of column dust optical depth around the storm bulk. Such degeneracy does not significantly affect the surface and air temperatures retrievals.

The degeneracy of aerosols content retrieval does not interfere with observing the thermal structure within the sensitivity of the nadir mode of viewing by the TIRVIM instrument. The advantage of TIRVIM is that the spectrometer is able to track the evolution of the mean meridional air temperature field twice a day throughout the storm due to the dense coverage of measurements instead of capturing just its initial and final states. Well-known equinoctial (fall season in the northern hemisphere) daytime and nighttime mean meridional thermal structures of Martian atmosphere are observed before the GDS. The Hadley circulation with nearly symmetric cells around the equator at this season leads to a dynamical "polar warmings" ≈170 K in the tropopause of both hemispheres and to cold "polar vortices" ≈150 K in the troposphere below. The semidiurnal difference between day and night mean meridional temperature fields reflects a well-known nodal pattern of vertically propagating diurnal thermal tide typical for the equinox with 5–10 K amplitudes. At the onset of the storm until $L_s = 191°$ the atmospheric dust dominated at equatorial and northern latitudes absorbs solar radiation during the day which causes heating of the daytime northern troposphere. The upward spreading of the temperature by descending branches of Hadley circulation also heats the tropopausal "polar warmings."

After the break of measurements the morning and evening mean meridional temperature fields demonstrate further heating of the atmosphere at the peak of the GDS. The opposite times a day thermal structures become very dissimilar compared to the usual equinoctial structures before the storm. The evening thermal structure reflects the latitudinal asymmetry in the heating of the atmosphere caused by dust particles daytime absorption of solar radiation with heavy dust loading dominated south than 40°N and as a result hotter southern troposphere with local maxima of 240–250 K. The reinforced Hadley circulation at nighttime transports hot air from the lower troposphere into the tropopause in both hemispheres which heats both "polar warmings" up to 200 K and southern "polar vortex" up to 180 K and also shifts equatorial local temperature maximum upward from the surface up to 15 km. As a result, significant heating during the GDS is observed in the middle troposphere and above, as well as in the southern hemisphere, which is especially evident for the daytime structure with total air heating up to 80 K at southern middle and polar latitudes. Nighttime heatings up to 40–50 K are detected in the tropopause of both hemispheres. The diurnal contrast of the atmospheric temperature also significantly changes during the storm due to the migrating diurnal tide, becoming much more asymmetric with day warmer than night. The region with strongest amplitudes up to 30 K is observed in the southern middle troposphere. Temperature deviations in the northern hemisphere are represented by the zone at mid-latitudes at 20 km with 15 K amplitudes and the tropopausal region at tropical latitudes with amplitudes of 10 K. In general, thermal effects caused by heavy dust presence in the atmosphere significantly dominate over ones caused by regular seasonal changing of circulation. The agreement of obtained results with

MCS/MRO observations is good and does not exceed the order of temperature retrieval errors taking into account low sensitivity at altitudes above 40 km and at polar latitudes with cold surface.

Massive injection of dust particles absorbing solar radiation has also caused a significant decrease of the mean daytime surface temperature by 20–50 K in general and up to 60 K in some regions. On the other hand, an increased backscattering of surface thermal emission from atmospheric dust particles reduced cooling of the surface after the sunset and led to a heating of the mean nighttime surface temperature by 10–30 K on average with a maximum of 45 K between 60°S and 35°N. Locations with the greatest relative nighttime warming coincide with regions with the coldest nighttime surface in dust-free atmosphere since they are determined by surface radiative properties more than by atmospheric dust loading. The obtained results are in good agreement with Curiosity rover measurements in the Gale Crater and GCM simulations assimilated with global column dust spatial distribution from MCS observations. But a correlation of the daytime cooling with daily averaged column dust spatial distribution is not observed and the retrieved surface temperature drop is ~20 K stronger on average than simulated with GCM.

Data Availability Statement

Raw ACS TIRVIM data are available from ESA's Planetary Science Archive at https://archives.esac.esa.int/psa/#!Table%20View/TIR=instrument. Processed spectra and retrieved data from TIRVIM nadir measurements during the GDS of MY 34 in the period from 26 May 2018 till 15 July 2018 (from L_s = 182.2° to 211.8°) are available in netCDF format from Vlasov (2022).

Acknowledgments
ExoMars is a space mission of European Space Agency and Roscosmos. The ACS experiment is led by IKI, the Space Research Institute in Moscow, assisted by LATMOS in France. The science operations of ACS are funded by Roscosmos and ESA. Data processing and analysis in IKI are funded by the Russian Science Foundation grant number 20-42-09035. S. Guerlet, F. Forget and E. Millour acknowledge support from the French CNES. The contribution of D. Grassi is supported by the Italian Space Agency through grant number 2018-2-HH.0.

References

Aoki, S., Vandaele, A. C., Daerden, F., Villanueva, G. L., Liuzzi, G., Thomas, I. R., et al. (2019). Water vapor vertical profiles on Mars in dust storms observed by TGO/NOMAD. *Journal of Geophysical Research: Planets*, *124*, 3482–3497. https://doi.org/10.1029/2019JE006109

Cantor, B. A. (2007). MOC observations of the 2001 Mars planet-encircling dust storm. *Icarus*, *186*(1), 60–96. https://doi.org/10.1016/j.icarus.2006.08.019

Clancy, R. T., Wolff, M. J., & Christensen, P. R. (2003). Mars aerosol studies with the MGS TES emission phase function observations: Optical depths, particle sizes, and ice cloud types versus latitude and solar longitude. *Journal of Geophysical Research*, *108*(E9), 5098. https://doi.org/10.1029/2003JE002058

Fedorova, A. A., Montmessin, F., Korablev, O., Luginin, M., Trokhimovskiy, A., Belyaev, D. A., et al. (2020). Stormy water on Mars: The distribution and saturation of atmospheric water during the dusty season. *Science*, *367*(6475), 297–300. https://doi.org/10.1126/science.aay9522

Forget, F., Hourdin, F., Fournier, R., Hourdin, C., Talagrand, O., Collins, M., et al. (1999). Improved general circulation models of the Martian atmosphere from the surface to above 80 km. *Journal of Geophysical Research*, *104*(E10), 24155–24175. https://doi.org/10.1029/1999JE001025

French, R. G., & Gierasch, P. J. (1979). The Martian polar vortex: Theory of seasonal variation and observations of Eolian features. *Journal of Geophysical Research*, *84*(B9), 4634–4642. https://doi.org/10.1029/JB084iB09p04634

Giuranna, M., Wolkenberg, P., Grassi, D., Aronica, A., Aoki, S., Scaccabarozzi, D., et al. (2021). The current weather and climate of Mars: 12 years of atmospheric monitoring by the Planetary Fourier Spectrometer on Mars Express. *Icarus*, *353*, 113406. https://doi.org/10.1016/j.icarus.2019.113406

Grassi, D., Fiorenza, C., Zasova, L. V., Ignatiev, N. I., Maturilli, A., Formisano, V., & Giuranna, M. (2005). The Martian atmosphere above great volcanoes: Early planetary Fourier spectrometer observations. *Planetary and Space Science*, *53*(10), 1053–1064. https://doi.org/10.1016/j.pss.2005.02.008

Guzewich, S. D., Lemmon, M., Smith, C. L., Martínez, G., de Vicente-Retortillo, Á., Newman, C. E., et al. (2019). Mars Science Laboratory observations of the 2018/Mars year 34 global dust storm. *Geophysical Research Letters*, *46*(1), 71–79. https://doi.org/10.1029/2018GL080839

Guzewich, S. D., Wilson, R. J., McConnochie, T. H., Toigo, A. D., Banfield, D. J., & Smith, M. D. (2014). Thermal tides during the 2001 Martian global-scale dust storm. *Journal of Geophysical Research: Planets*, *119*, 506–519. https://doi.org/10.1002/2013JE004502

Kass, D. M., Schofield, J. T., Kleinböhl, A., McCleese, D. J., Heavens, N. G., Shirley, J. H., & Steele, L. J. (2019). Mars Climate Sounder observation of Mars' 2018 global dust storm. *Geophysical Research Letters*, *46*(23), e2019GL083931. https://doi.org/10.1029/2019GL083931

Kleinböhl, A., Schofield, J. T., Kass, D. M., Abdou, W. A., Backus, C. R., Sen, B., et al. (2009). Mars Climate Sounder limb profile retrieval of atmospheric temperature, pressure, and dust and water ice opacity. *Journal of Geophysical Research*, *114*, E10006. https://doi.org/10.1029/2009JE003358

Kleinböhl, A., Spiga, A., Kass, D. M., Shirley, J. H., Millour, E., Montabone, L., & Forget, F. (2020). Diurnal variations of dust during the 2018 global dust storm observed by the Mars Climate Sounder. *Journal of Geophysical Research: Planets*, *125*, e2019JE006115. https://doi.org/10.1029/2019JE006115

Korablev, O., Montmessin, F., Trokhimovskiy, A., Fedorova, A. A., Shakun, A. V., Grigoriev, A. V., et al. (2018). The atmospheric chemistry suite (ACS) of three spectrometers for the ExoMars 2016 trace gas orbiter. *Space Science Reviews*, *214*(1), 7. https://doi.org/10.1007/s11214-017-0437-6

Lee, C., Lawson, W. G., Richardson, M. I., Heavens, N. G., Kleinböhl, A., Banfield, D., et al. (2009). Thermal tides in the Martian middle atmosphere as seen by the Mars Climate Sounder. *Journal of Geophysical Research*, *114*, E03005. https://doi.org/10.1029/2009JE003285

Luginin, M., Fedorova, A., Ignatiev, N., Trokhimovskiy, A., Shakun, A., Grigoriev, A., et al. (2020). Properties of water ice and dust particles in the atmosphere of Mars during the 2018 global dust storm as inferred from the atmospheric chemistry suite. *Journal of Geophysical Research: Planets*, *125*, e2020JE006419. https://doi.org/10.1029/2020JE006419

Martin, L. J., & Zurek, R. W. (1993). An analysis of the history of dust activity on Mars. *Journal of Geophysical Research*, *98*(E2), 3221–3246. https://doi.org/10.1029/92JE02937

Martin, T. Z., & Kieffer, H. H. (1979). Thermal infrared properties of the Martian atmosphere, 2: The 15 μm band measurements. *Journal of Geophysical Research*, *84*(B6), 2843–2852. https://doi.org/10.1029/JB084iB06p02843

Martin, T. Z., Peterfreund, A. R., Miner, E. D., Kieffer, H. H., & Hunt, G. E. (1979). Thermal infrared properties of the Martian atmosphere 1. Global behavior at 7, 9, 11, and 20 μm. *Journal of Geophysical Research*, *84*(B6), 2830–2842. https://doi.org/10.1029/JB084iB06p02830

McCleese, D. J., Heavens, N. G., Schofield, J. T., Abdou, W. A., Bandfield, J. L., Calcutt, S. B., et al. (2010). Structure and dynamics of the Martian lower and middle atmosphere as observed by the Mars Climate Sounder: Seasonal variations in zonal mean temperature, dust, and water ice aerosols. *Journal of Geophysical Research*, *115*, E12016. https://doi.org/10.1029/2010JE003677

Montabone, L., Spiga, A., Kass, D. M., Kleinboehl, A., Forget, F., & Millour, E. (2020). Martian year 34 column dust climatology from Mars Climate Sounder observations: Reconstructed maps and model simulations. *Journal of Geophysical Research: Planets*, *125*, e2019JE006111. https://doi.org/10.1029/2019JE006111

Revercomb, H. E., Buijs, H., Howell, H. B., LaPorte, D. D., Smith, W. L., & Sromovsky, L. A. (1988). Radiometric calibration of IR Fourier transform spectrometers: Solution to a problem with the High-Resolution Interferometer Sounder. *Applied Optics*, *27*(15), 3210–3218. https://doi.org/10.1364/AO.27.003210

Santee, M., & Crisp, D. (1993). Thermal structure and dust loading of the Martian atmosphere during late southern summer: Mariner 9 revisited. *Journal of Geophysical Research*, *98*(E2), 3261–3279. https://doi.org/10.1029/92JE01896

Shakun, A., Ignatiev, I., Luginin, M., Grigoriev, A., Moshkin, B., Grassi, D., et al. (2018). ACS/TIRVIM: Calibration and first results. In *Infrared remote sensing and instrumentation XXVI* (p. 107650E). SPIE. https://doi.org/10.1117/12.2322163

Shirley, J. H. (2015). Solar System dynamics and global-scale dust storms on Mars. *Icarus*, *251*, 128–144. https://doi.org/10.1016/j.icarus.2014.09.038

Shirley, J. H., Kleinböhl, A., Kass, D. M., Steele, L. J., Heavens, N. G., Suzuki, S., et al. (2019). Rapid expansion and evolution of a regional dust storm in the Acidalia Corridor during the initial growth phase of the Martian global dust storm of 2018. *Geophysical Research Letters*, *46*(9), e2019GL084317. https://doi.org/10.1029/2019GL084317

Smith, M. D. (2004). Interannual variability in TES atmospheric observations of Mars during 1999–2003. *Icarus*, *167*(1), 148–165. https://doi.org/10.1016/j.icarus.2003.09.010

Smith, M. D. (2019). THEMIS observations of the 2018 Mars Global Dust Storm. *Journal of Geophysical Research: Planets*, *124*, 2929–2944. https://doi.org/10.1029/2019JE006107

Smith, M. D., Bandfield, J. L., Christensen, P. R., & Richardson, M. I. (2003). Thermal Emission Imaging System (THEMIS) infrared observations of atmospheric dust and water ice cloud optical depth. *Journal of Geophysical Research*, *108*(E11), 5115. https://doi.org/10.1029/2003JE002115

Streeter, P. M., Lewis, S. R., Patel, M. R., Holmes, J. A., & Kass, D. M. (2020). Surface warming during the 2018/Mars year 34 global dust storm. *Geophysical Research Letters*, *47*(9), e2019GL083936. https://doi.org/10.1029/2019GL083936

Vago, J., Witasse, O., Svedhem, H., Baglioni, P., Haldemann, A., Gianfiglio, G., et al. (2015). ESA ExoMars program: The next step in exploring Mars. *Solar System Research*, *49*(7), 518–528. https://doi.org/10.1134/S0038094615070199

Vlasov, P. (2022). *Thermal structure of the Martian atmosphere and dust content from ACS TIRVIM nadir measurements during the GDS of MY 34*. Mendeley Data, V2. https://doi.org/10.17632/35y8775x5z.2

Wilson, R. J., & Richardson, M. I. (2000). The Martian atmosphere during the Viking mission I: Infrared measurements of atmospheric temperatures revisited. *Icarus*, *145*(2), 555–579. https://doi.org/10.1006/icar.2000.6378

Wolff, M. J., & Clancy, R. T. (2003). Constraints on the size of Martian aerosols from Thermal Emission Spectrometer observations. *Journal of Geophysical Research*, *108*(E9), 5097. https://doi.org/10.1029/2003JE002057

Wolkenberg, P., & Giuranna, M. (2021). Daily dust variation from the PFS MEx observations. *Icarus*, *353*, 113823. https://doi.org/10.1016/j.icarus.2020.113823

Wolkenberg, P., Giuranna, M., Smith, M. D., Grassi, D., & Amoroso, M. (2020). Similarities and differences of global dust storms in MY 25, 28, and 34. *Journal of Geophysical Research: Planets*, *125*, e2019JE006104. https://doi.org/10.1029/2019JE006104

Zasova, L., Formisano, V., Grassi, D., Ignatiev, N., & Maturilli, A. (2002). Martian winter atmosphere at North high latitudes: Mariner 9 IRIS data revisited. *Advances in Space Research*, *29*(2), 151–156. https://doi.org/10.1016/S0273-1177(01)00563-4

Zasova, L., Grassi, D., Formisano, V., & Maturilli, A. (2001). The Martian atmosphere in the region of the great volcanoes: Mariner 9 IRIS data revisited. *Planetary and Space Science*, *49*, 977–992. https://doi.org/10.1016/S0032-0633(01)00040-X

References From the Supporting Information

Conrath, B. J., Pearl, J. C., Smith, M. D., Maguire, W. C., Christensen, P. R., Dason, S., & Kaelberer, M. S. (2000). Mars Global Surveyor Thermal Emission Spectrometer (TES) observations: Atmospheric temperatures during aerobraking and science phasing. *Journal of Geophysical Research*, *105*(E4), 9509–9519. https://doi.org/10.1029/1999JE001095

Gordon, I. E., Rothman, L. S., Hargreaves, R. J., Hashemi, R., Karlovets, E., Skinner, F., et al. (2022). The HITRAN2020 molecular spectroscopic database. *Journal of Quantitative Spectroscopy and Radiative Transfer*, *277*, 107949. https://doi.org/10.1016/j.jqsrt.2021.107949

Guerlet, S., Ignatiev, N., Forget, F., Fouchet, T., Vlasov, P., Bergeron, G., et al. (2022). Thermal structure and aerosols in Mars' atmosphere from TIRVIM/ACS onboard the ExoMars Trace Gas Orbiter: Validation of the retrieval algorithm. *Journal of Geophysical Research: Planets*, *127*, e2021JE007062. https://doi.org/10.1029/2021JE007062

Millour, E., Forget, F., Spiga, A., Vals, M., Zakharov, V., & Montabone, L. (2018). MCD/GCM Development team. In *The Mars climate database (version 5.3). From Mars Express to ExoMars Scientific Workshop* (p. 2). ESA-ESAC Madrid. 27–28 February.

Rodgers, C. D. (1976). Retrieval of atmospheric temperature and composition from remote measurements of thermal radiation. *Reviews of Geophysics and Space Physics*, *14*(4), 609–624. https://doi.org/10.1029/RG014i004p00609

Rodgers, C. D. (2000). *Inverse methods for atmospheric sounding: Theory and practice*. World Scientific. https://doi.org/10.1142/3171

Smith, M. D., Bandfield, J. L., & Christensen, P. R. (2000). Separation of atmospheric and surface spectral features in Mars Global Surveyor Thermal Emission Spectrometer (TES) spectra. *Journal of Geophysical Research*, *105*(E4), 9589–9607. https://doi.org/10.1029/1999JE001105

Erratum

In the caption for figure 2, "Thermal InfraRed channel Vassili Ivanovich Moroz" was changed to "Thermal InfraRed channel in honor of professor Vassili Ivanovich Moroz (TIRVIM)." In the second paragraph of Section 4, "reaching ≈ of zonal mean" was changed to "reaching ≈1 of zonal mean." This version may be considered the authoritative version of record.